Lattice preferred orientation of talc and implications for seismic anisotropy in subduction zones

Jungjin Lee,[1] Haemyeong Jung,[1*] Reiner Klemd,[2] Matthew S. Tarling,[3] Dmitry Konopelko[4,5]

[1] School of Earth and Environmental Sciences, Seoul National University, Seoul, Republic of Korea. [2] GeoZentrum Nordbayern, Universität Erlangen, Schlossgarten 5a, Erlangen, Germany. [3] Geology Department, University of Otago, Dunedin, New Zealand. [4] Department of Regional Geology, St. Petersburg State University, University Embankment, St. Petersburg, Russia. [5] Novosibirsk State University, 2 Pirogova St. Novosibirsk, Russia.

Introduction

Seismic anisotropy is generally observed in subduction zones. Lattice preferred orientation (LPO) of minerals has been considered to be important factor causing seismic anisotropy. Talc is one of the mechanically weakest minerals on Earth and has been reported to be formed In the slab and slab-mantle interfaces by various processes. Here, we report on measured LPOs of polycrystalline talc in talc-rich schist samples collected from metasomatic and ultrahigh-pressure metamorphic complexes. We also provide evidence for its significant contribution to radial and azimuthal P-wave anisotropy and trench-parallel S-wave seismic anisotropy in subduction zones.

Geological setting of the samples

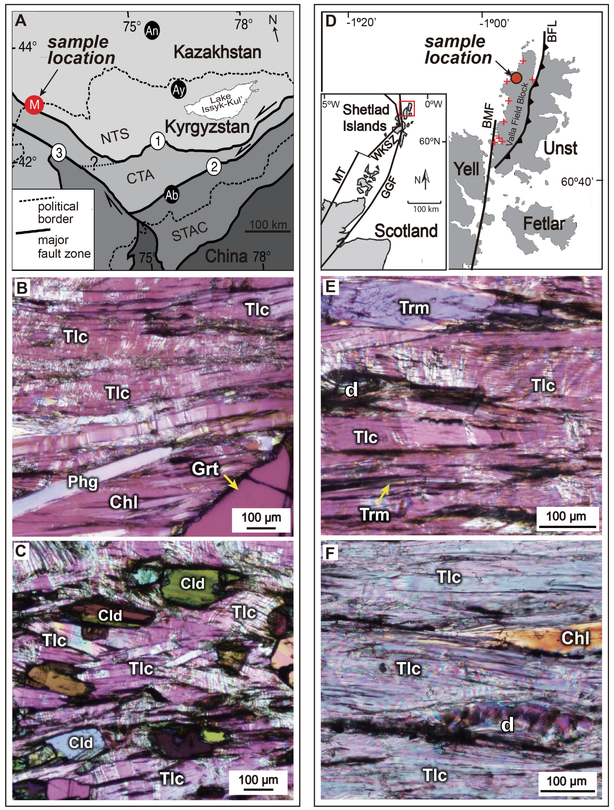

Figure 1. (A) Sample locations of Makbal UHP talc schists. **(B,C)** Microphotograph of the ultramafic schist samples 10–16 **(B)** 12–52 **(C)**. **(D)** Sample location of Unst metasomatic talc schists. **(E,F)** Microphotographs of the Unst metasomatic schist samples UN04 **(E)** UN22 **(F)**. Tlc, talc; Trm, tremolite; Chl, chlorite; and d, depression.

LPOs of talc and seismic anisotropy of talc

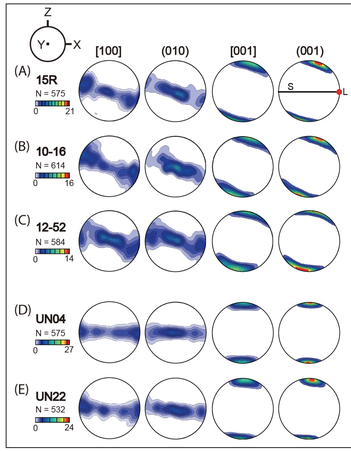

Figure 2. Pole figures of polycrystalline talc **(A – E)**. **(A, B and C)** Samples from UHP Makbal Complex. **(D, E)** Samples from Valla Complex in Unst. Pole figures are presented in lower hemisphere using an equal-area projection. N; the number of analyzed grains. Colorbars indicate LPO strengths in units of multiples of random distribution (m.r.d.). X-direction is parallel to the lineation (L), Z–direction normal to the foliation (S), and Y-direction orthogonal to the X-Z plane.

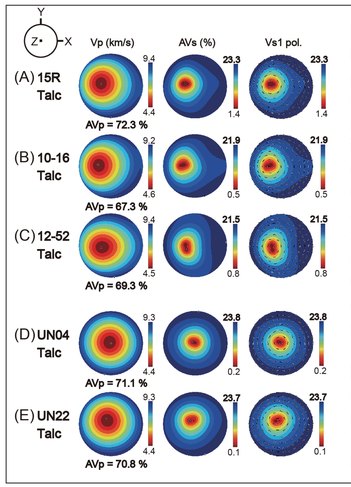

Figure 3. P-wave velocity, P-wave azimuthal anisotropy, S-wave anisotropy and fast S-wave polarization direction of polycrystalline talc in each sample **(A – E)**. Vp (km/s): P-wave velocity, AVp (%): anisotropy of P-wave, AVs (%): anisotropy of S-wave, Vs1 pol.: polarization direction of fast S-wave. Colorbars inidcate Vp (km/s) in the first column and AVs (%) in the second and last column, respectively. X-direction is parallel to the lineation (L), Z-direction normal to the foliation (S), and Y-direction perpendicular to the X-Z plane.

Implications for seismic anisotropy in subduction zones

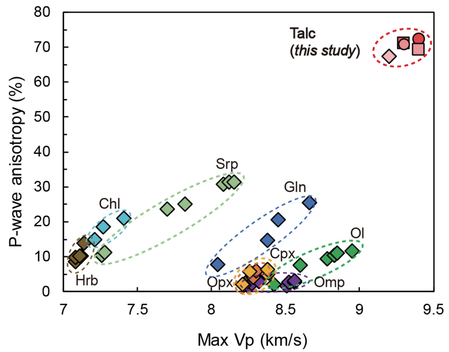

Figure 4. Comparison of the P–wave anisotropy of talc aggregates with that of other polycrystalline minerals. The P–wave anisotropy (AVp) data of polycrystalline minerals were obtained from natural samples and combined with data of their maximum P–wave velocities (Vp). Talc in this study is denoted by the reddish color shapes. Ol, olivine (Park and Jung, 2015); Opx, orthopyroxene (Jung et al., 2010); Cpx, clinopyroxene (Park and Jung, 2015); Gln, glaucophane (Cao et al., 2013); Omp, omphacite (Cao et al., 2013; Kim et al., 2016); Srp, serpentine (Hirauchi et al., 2010; Jung, 2011; Watanabe et al., 2014); Chl, chlorite (Kim and Jung, 2015); and Hrb, hornblende (Ji et al., 2013).

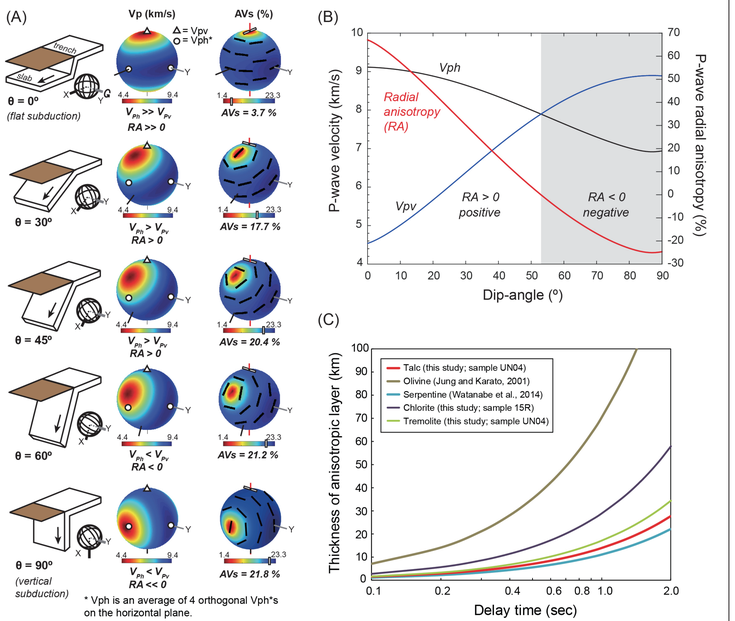

Figure 5. (A) P–wave velocity (Vp) and S–wave anisotropy (AVs) of talc aggregates in 3-D considering the dip-angle (θ) of the subducting slab. LPOs of talc in Fig. 2 (sample 15R for Vp and sample UN04 for AVs, respectively) were used. Square dots denote vertical P–wave velocity (Vpv) and round dots show two of the four orthogonal P–wave velocities on the horizontal plane (Vph*) which were averaged to define the horizontal P–wave anisotropy (Vph). **(B)** Variations of Vph, Vpv and radial anisotropy (RA) with changes in slab dip-angle. Grey color area indicates the dip-angle ranges for the RA < 0. **(C)** Thickness of anisotropic layer (L) as a function of delay time (dt) of S–wave. The used AVs of talc is 23.8 % (sample UN04 from this study), of olivine 4.9 % (Jung and Karato, 2001), of serpentine 25.0 % (Watanabe et al., 2014), of chlorite (sample 15R from this study) and of tremolite (sample UN04 from this study).

Method

LPOs of talc were measured by using JEOL JSM-6380 SEM with HKL EBSD at Seoul National University. Seismic anisotropy was calculated as

$$AVp\ (\%) = \frac{Vp_{max} - Vp_{min}}{(Vp_{max} + Vp_{min})/2} \times 100 \qquad AVs\ (\%) = \frac{Vs_1 - Vs_2}{(Vs_1 + Vs_2)/2} \times 100$$

$$RA = (Vph - Vpv) / \{(Vph + Vpv)/2\}$$

where Vph is the average velocity of horizontally propagating P–waves and Vpv is the vertically propagating P–wave velocity.

References

Please see the published version of this work (Lee et al., 2020, *EPSL*, 537, 116178. doi.org/10.1016/-j.epsl.2020.116178).

Conclusion

LPOs of polycrystalline talc were measured in natural rock samples which include a strong LPO showing a strong alignment of (001) planes subparallel to the foliation and a girdle distribution of [100] axes and (010) poles subparallel to the foliation. The seismic anisotropy results of polycrystalline talc suggest that the strong LPO of talc significantly contribute to the production of seismic anisotropies of both P–waves and S–waves in subduction zones.